This is the accepted manuscript made available via CHORUS. The article has been published as:

Simulating liquid and amorphous silicon dioxide using real-space pseudopotentials

Minjung Kim, K. H. Khoo, and James R. Chelikowsky

Phys. Rev. B **86**, 054104 — Published 2 August 2012

DOI: 10.1103/PhysRevB.86.054104

Simulating liquid and amorphous silicon dioxide using real-space pseudopotentials

Minjung Kim
Department of Chemical Engineering, The University of Texas at Austin, Austin, Texas 78712, USA

K. H. Khoo
Department of Materials Science and Engineering,
Institute of High Performance Computing, Singapore 138632, Singapore

James R. Chelikowsky
Center for Computational Materials, Institute for Computational Engineering and Sciences
Departments of Physics and Chemical Engineering,
The University of Texas at Austin, Austin, Texas 78712, USA

(Dated: June 26, 2012)

We present *ab initio* molecular dynamics simulations of liquid and amorphous silicon dioxide. The interatomic forces in our simulations are calculated using real-space pseudopotentials, which were constructed using density-functional theory. Our simulations are carried out using Born-Oppenheimer molecular dynamics, *i.e.*, the electronic structure problem is solved by performing fully self-consistent calculations for each time step. Using a subspace filtering iteration technique, we avoid solving the Kohn-Sham eigenvalue with "standard" diagonalization methods. We consider systems with up to 192 atoms (64 SiO_2 units) in a periodic supercell for simulations over 20 ps. The liquid and amorphous ensembles are formed by thermally quenching random configurations of silicon and oxygen atoms. We compare our liquid and amorphous simulations with previously performed Car-Parrinello molecular dynamic simulations and with experiment. In particular, we examine the possible formation of two-fold rings, which were not observed in previous simulations using quantum forces. We attribute this difference to a "biased" initial configuration, which inhibits the formation of two-fold rings. We also compare the structural properties of our simulated amorphous systems with neutron diffraction measurements and find good agreement.

I. INTRODUCTION

Silicon dioxide is a very abundant material on earth's crust. Forms of silica exist in many allotrope forms with varying temperature and pressure conditions. Because of this, silica has been considered as a fundamental oxide system and as an archetype of tetrahedral structures, which are thought to include amorphous, and liquid phases. During the last few decades, silica has played a crucial role in development of electronic devices and technologies. For example, amorphous silica is commonly used in electronic devices such as MOSFET as a dielectric material, as it forms an electronically passive interface with silicon and can be precisely patterned in the construction of nano-scale devices. Silica also is used in optical fibers as a transparent material.[1,2]

Owing to the fundamental importance of silica in earth and materials science, and its many technological uses, numerous studies of silica structures have been carried out, both theoretical and experimental. In contrast to the well-defined structural properties of crystalline forms,[3] structural details of amorphous and liquid silica are problematic. For instance, the details of Si-O-Si bond angle distributions of amorphous silica obtained from various experiments using x-ray, neutron diffraction, and NMR analysis are not in general agreement with recent simulations.[4]

In order to clarify the structural and dynamical properties, many theoretical models of amorphous (a)- and liquid (l)- SiO_2 have been proposed. These models were generated by different simulation techniques: classical and *ab initio* molecular dynamics, Monte-Carlo, and cluster simulations.[5–7] Among these different simulations, *ab intio* molecular dynamics simulations employing periodic boundary conditions are the most accurate as they reflect the quantum nature of the interatomic forces. As such, they more accurately represent changes in hybridization and charge transfer effects as bonds break and reform in dynamical simulations.

A chief drawback of *ab initio* simulations is that they are computationally intensive and often limited by computational constraints to relatively small systems and short simulation times when compared to simulations using interatomic potentials based on fits to experiment. Previous of the a-SiO_2 simulations were conducted for systems less than hundred atoms[8–11] with a quenching rate that remained around 10^{15} K/s. It has been reported that while the short range of interactions are not sensitively affected by periodic constraints, medium or long range interactions such as ring statistics are sensitive to the size of the ensemble.[12] Of course, short cooling rates can also change the structural properties of amorphous silica.[13]

In order to mitigate computational limitations for *ab initio* simulations, we have developed algorithms to reduce the computational load associated with solving the eigenvalue problem at each time step.[14,15] We have successfully applied these algorithms to liquid Al and $Al_{1-x}Si_x$ alloy system with five hundred atoms.[16,17] Here, we use the same approach for SiO_2 systems containing up to 192 atoms. We present liquid simulations and then consider quenching the liquid ensemble to model amorphous solids. We compare structural and dynamical properties for the liquid with other classical and *ab initio* molecular dynamics simulations. For amorphous silica, we investigate structural properties of the amorphous state and compare to previous simulations and experiments.

II. COMPUTATIONAL DETAILS

All calculations we performed are based on density functional theory combined with real-space pseudopotentials.[18] Within the real-space formalism, an explicit basis is not required. Convergence is determined by a single parameter for a cubic grid, *i.e.*, the grid spacing. We use a grid spacing of 0.35 a.u. (1 a.u. = 0.5291 Å) for our simulations, which corresponds to a ∼60 Ry plane wave cutoff. For structural properties of amorphous silica, we use a finer grid with a spacing of 0.30 a.u. to obtain highly accurate forces. We carry out our simulations in a cubic supercell containing 192 atoms or 64 molecular units of SiO_2. We assume the experimental density of amorphous silica ($2.2 g/cm^3$) as is often done to fix the size of the cell.[11] This constraint yields a cell edge size of 27.0 a.u. We keep the density constant during entire simulations, which implies a change in pressure as the temperature of the cell is altered. This is a small effect compared to other uncertainties, *e.g.*, the use of density functional theory.

We employ norm-conserving pseudopotentials with a $3s^23p^2$ atomic configuration for silicon and $2s^22p^4$ for oxygen. The silicon ionic pseudopotential was generated with a 2.5 a.u. cutoff radii for both the s and p potentials, and the s potential was chosen as the local component. For the oxygen ionic pseudopotential, a cutoff radius of 1.45 a.u. was applied for both s and p potentials with the p potential taken as the local component. We use the local density approximation for exchange-correlation functional from Ceperley and Alder.[19] Since the periodicity of the supercell has no physical meaning in our simulation, we do not consider a sampling over different $\vec{k}$-points and consider only the $\vec{k} = 0$ point. Provided the cell size is sufficiently large, this should be an accurate approximate.

We generate amorphous structures using simulated annealing.[20,21] Typically, simulated annealing employs three steps. First, in order to randomize the initial coordinates of atoms, the system is heated to a very high temperature, *i.e.*, well above the melting point of the silica. Second, the system is "slowly" cooled to a targeted temperature. Third, data is collected from a microcanonical simulations using Newtonian dynamics. We chose a Langevin equation

of motion as a temperature thermostat. The trajectories of the atomic species are

$$M_i \frac{d\vec{v}_i}{dt} = -\gamma M_i \vec{v}_i + \vec{G}_i(\gamma, T) + \vec{F}_i, \tag{1}$$

where M_i is the atomic mass of the ith species, γ is a viscosity or friction coefficient, and G is a random force appropriate for a heat bath of temperature T.[20,22] A time step of 165 a.u. (4 fs) was applied with the friction coefficient of 0.002 Ry/$\hbar$. Fig. 1 illustrates the details of our annealing schedule. We note that our annealing rate, 2.5×10^{14} K/s, is significantly slower than the previous *ab initio* simulations (10^{15} K/s (Ref. 11), and 9×10^{14} K/s (Ref. 8)).

Various annealing schedules have been applied to previous simulations.[8,11,13,23] As a starting point, both crystalline and random configurations of atoms can be used. We used β-cristobalite as a starting point and set our initial temperature to be 5,000 K. β-cristobalite is a high temperature form of crystalline silica that can be constructed by considering a diamond crystal of silicon and placing oxygen atoms at the bond sites. By using this form as a starting point, we can avoid unrealistically high energy configurations that might occur by a random placement of atomic species. We considered initial temperatures up to 7,000 K to randomize the initial geometry.[23] We found that 5,000 K is sufficient to randomize the crystalline structure and remove any memory of the original state. Previous Car-Parrinello molecular dynamics simulations used atomic coordinates generated by empirical potential simulations and set the initial temperature at 3,500 K.[8] Our experience is that defects existing in the initial structure, cannot be removed by annealing even at this relatively high temperature.

The mean square displacement shown in Fig. 1 was determined from

$$\frac{1}{N_\alpha} \sum_i \left[\mathbf{R}_{\alpha i}(t) - \mathbf{R}_{\alpha i}(t=0)\right]^2 \tag{2}$$

where N_α is the number of atom species α in the supercell. The average displacement during the entire simulation was 4.5 Å for Si and 5.1 Å for O. This displacement is significantly larger than the Si-Si and O-O bond lengths from the initial crystal structure: the bond lengths are 3.09 Å and 2.52 Å, respectively. Displacements of this length ensure that the initial structure is sufficiently randomized to remove correlations with the initial crystal structure.

III. LIQUID SIMULATION

Fig. 1 shows an annealing schedule for the simulation for an initial temperature of 5,000 K and a final temperature of 300 K. Also shown is the mean square displacement of the atomic species. Most changes in the mean square displacement occur in high temperature region where the ensemble is removed from equilibrium. The parabolic shape for the initial stage of the simulation is expected for ballistic trajectories as the system has yet to thermalize. The linear regime for the first 5-6 ps represents a liquid state. From 5 to 10 ps, the steepness of the slope is gradually decreased as the system attempts to solidify. After 10 ps, there is no significant changes in the mean square displacement other than the fluctuation. In order to study the temperature dependence of structural and dynamical properties, we performed two liquid simulations at different temperatures.

To prepare the liquid, we extracted two snapshots at 3,000 K and 3,500 K then ran extra 2 ps for each simulation simultaneously. The average temperatures of liquid were 3,120 K and 3,700 K, respectively. These temperatures are well above the experimental melting point of silica (∼2,000 K) and ensures that we are well within the liquid regime. It is a problematic issue as to when "density functional" silica will melt, but the nature of the mean square displacement in Fig. 1 indicates solidification should not occur below these temperatures. Previous simulations have also used this temperature region for liquid simulations.[8,24]

For the liquid state, we determined the pair correlation function and show our results in Fig. 2. There are small changes in peak position and peak height between the two temperature regimes. The first peak height of Si-O bond length increases by ∼10 %, and the entire first peak of Si-Si had been shifted towards shorter distance by about 0.1 Å as the temperature is decreased. Detailed values of the peak positions are given in Table. I, and corresponding values of amorphous and β-cristobalite are also given in the same table.

Even though only small changes were observed in partial pair correlation function, Fig. 3 shows significant differences in the Si-O-Si bond angle distribution function between two simulations. The angle distributions for Si-O-Si and O-Si-O are shown. The O-Si-O angle represents a tetrahedral angle (109.5°) for crystalline silicon whereas the Si-O-Si shows strong variations in the crystalline structure, depending on the silica polytype. Typically the Si-O-Si bond is ∼140° as in quartz. In idealized β-cristobalite, it is 180°. The difference in the distribution occurs for the Si-O-Si when the bond angle is smaller than 100°. The simulation for the liquid at 3,120 K shows a pronounced peak around 90°, but it is not shown in the 3,700 K simulation. In previous simulations performed for a-SiO_2 simulations, the

peak between 80-100° was regarded as evidence for the existence of two-membered ring.[11] Fig. 3 indicates that the existence of a two-membered ring was not excluded during the cooling process from 3,700 K to 3,120 K.

In order to understand coordination changes in configurations at different temperatures, we examined coordination number as a function of coordination radius in Fig. 4. At high temperatures, Si and O atoms are often miscoordinated. For example, 20 % of Si atoms are coordinated with only three O atoms even at the 2 Å coordination radius, and few Si atoms are coordinated with five O atoms at 3,700 K. However, these coordination errors were significantly reduced at 3,120 K. We also display results from simulations using Car-Parrinello molecular dynamics (CPMD)[8] for comparison. The temperature for the CPMD simulation as taken to be 3,500 K. Their coordination number statistics are similar to our simulation performed at 3,120 K.

Diffusion coefficients are an important measure for quantifying liquid behavior.[12] We employed the Einstein relation[25] to calculate diffusion constant:

$$D_\alpha = \lim_{t\to\infty} \frac{< [\mathbf{R}_\alpha (t)]^2 >}{6t} \tag{3}$$

The calculated diffusion constants for Si and O in liquid silica within the temperature range from 3,000 K to 3,700 K are tabulated in Table. II and also shown in Fig. 5 as are previous results. We also indicated the diffusion coefficient ratio between Si and O in Table. II. As is expected, the mobility of oxygen is always higher than silicon.

IV. AMORPHOUS STRUCTURE

To obtain statistical average for the amorphous structure, we carried out 400 steps of molecular dynamics simulations at 300 K. We compared several structural properties with experimental data and previously performed simulation results.

The total static structure factor of neutron scattering experiment is available for a-SiO_2.[26] Since silica is a heterogeneous system, the structure factor can be calculated by weighted sum of partial structure factors, $S_{\alpha\beta}$.

$$S(q) = \frac{\sum_{\alpha,\beta} b_\alpha b_\beta (c_\alpha c_\beta)^{1/2} [S_{\alpha\beta}(q) + 1]}{\sum_\alpha c_\alpha b_\alpha^2} \tag{4}$$

$c_{\alpha,\beta}$ is the concentration of silicon and oxygen, and $b_{\alpha,\beta}$ is a scattering length. (b_{Si}=4.149 fm, b_O= 5.803 fm). $S_{\alpha\beta}$ is obtained by a Fourier transform of the partial pair correlation function, $g_{\alpha\beta}$.

$$S_{\alpha\beta}(q) = \delta_{\alpha\beta} + 4\pi\rho (c_\alpha c_\beta)^{1/2} \int_0^\infty r^2 \frac{\sin(qr)}{qr} (g_{\alpha\beta}(r) - 1)\, dr \tag{5}$$

The structure factor only depends on the magnitude of wave vector $\mathbf{q}$ owing to the isotropic character of the amorphous systems. The calculated static structure factor fits very well with experimental data. (See Fig. 6) Our simulations accurately reproduce the position of the first three peaks in static structure factor. The partial pair correlation functions, $g_{\alpha\beta}(r)$, that were used in (5) are shown in Fig. 7.

We calculated the average values of bond angle and bond length in Table. III. For comparison, Car-Parinello MD and classical MD simulation results are also tabulated. Our simulation shows good agreement with experimental data. Details of short-range bond angle distributions, Si-O-Si and O-Si-O, are shown in Fig. 8. Previous CPMD results are indicated by a dashed line in the same figure. A noticeable difference between two simulations is a peak below 100° in the Si-O-Si bond angle distribution function. This peak suggests the existence of two-membered(2m) ring (an edge-sharing pair) as we noted in discussing our liquid simulations. The relatively small Si-O-Si angle comes from the geometry of a quadrangular configuration of the 2m ring as shown in Fig. 10. This peak also contributes to a slightly smaller value for average bond angle of Si-O-Si relative to experiments in Table. III, since even a single occurance of a 2m ring makes a considerable change the bond angle distribution function owing to the size of the supercell. The character of 2m ring structure is also detected in partial pair correlation function in Fig. 7. We note the small peak in $g_{SiSi}(r)$ around 2.4 Å, which is not shown in compared CPMD data. Typically, the distances between Si-Si of 2m rings is in range of 2.3 - 2.5 Å, which is comparable value to the small peak in $g_{SiSi}(r)$ figure.

Two-membered rings have been observed in some previous simulations[11,13]; however, these rings are absent in other simulations.[8,23] To understand the origin of these differences, we performed a variety of different preparations for our simulations, *i.e.*, we examined cells containing 8, 32, and 64 unit of SiO_2 with cooling rates ranging from 2.5×10^{14} to 10^{15}K/s. Among them, only the simulation for the 8 units of SiO_2 with a cooling rate of 2.5×10^{14}K/s did not result

in a 2m ring configuration. In general, increasing the size of the system allowed the two membered ring configuration even for the slowest cooling rate.

The same phenomenon was reported by Binder *et al.*[13] They tested several cooling rates with 1,002 atoms and the slowest cooling rate was 4.4×10^{12}K/s, which is two orders of magnitude slower than most *ab initio* simulations. Their study showed evidence for a 2m ring even for the slowest cooling rate.

In order to determine the possibility of existence of 2m ring in amorphous structures, we compared total energy of thirteen different systems prepared as mentioned above. We picked one snapshot in each simulation at 300 K and performed structural relaxation for each cell. Among them, we chose the lowest energy as the zero reference energy. We indicated total energy per atom instead of total energy since cells contain different number of atoms. The energy differences are not significant between the two simulation groups as illustrated in Fig. 9.

However, since the 2m ring population is a small fraction of the entire system, total energy comparisons may not accurately reflect the presence of 2m rings. Rather than performing total energy comparison of the entire cell, we attempted to examine the energy of the local structure. Extracting an energy representing a localized configuration is not a trivial exercise within density functional theory as contrasted with a classical simulation. We estimated the energy cost for a 2m ring and corner-sharing by considering clusters of bulk amorphous silica. Hydrogen was used to passivate our model clusters. We considered small clusters as it is shown in Fig. 10 and calculated the cohesive energy of two configurations labeled by (a) for a corner sharing geometry and (b) for a two membered ring cluster. In (a) clusters, the average value of cohesive energy was -6.17 eV/atom while for (b) clusters was -6.43 eV/atom, implying the 2m ring clusters are favorable structures compared to the corner-sharing clusters. To check the applicability of this approach to a bulk environment, we considered clusters with a second-shell of SiO_2 (Fig. 11). The cohesive energies of both (a) and (b) cluster in Fig. 11 were similar, that is -6.56 eV/atom for (a) and -6.52 eV/atom for (b). Adding second-shell atoms to the cluster results in reducing the energy difference. This explains why Fig. 9 does not show a difference in total energy between two groups and suggests that there is not a significant energy disadvantage of generating 2m rings in amorphous silica.

There could be an argument that a 2m ring may result in a large strain than larger rings, *e.g.*, three-membered or four-membered ring. However, previously performed simulations reported the calculated strain energies of 2m ring were in range of $1.23 \sim 1.85$ eV/Si_2O_4[27–29] which is smaller than formation energy of oxygen vacancies frequently observed in silica. Boureau *et al.*[30] discussed the thermodynamical lower bound of formation energy of β-cristobalite is 7.3 eV/defect and *ab initio* studies showed the formation energy is about $5 \sim 9$ eV/defect.[23,31,32] These values support the idea that the strain energy of 2m ring may not be a considerable barrier of generating this configuration in silica if one compares to the oxygen defects.

The formation of the 2m ring on silica surfaces has been also discussed in previous infrared studies.[33,44,45] In order to understand the vibrational spectrum of the 2m ring, we calculated the vibrational density of states with the 24-atom system. Figure 12 shows our calculations in comparison to the CPMD simulation (dashed line) and experiment (circles). The overall agreement with experiment is good despite the small simulation cell. The dotted line indicates the contribution of the 2m ring atoms which is extended in 200-1000 cm^{-1} range. Two distinctive and broad peaks between 250-450 and 700-900 cm^{-1} result from the 2m ring, and the position of these two peaks are similar to the previous theoretical calculations by Bendale and Hench[33], who showed several sharp peaks between 200-400 and 740-1100 cm^{-1}. In IR experiment on dehydroxylated a-SiO_2 surface, two unique peaks at 888 and 908 cm^{-1} have been reported.[44] These two peaks are regarded to be a strained defect, i.e., the edge-sharing structure on the surface. We note that the IR experiments focused on the surface that was thermally treated. Therefore, the population of the edge-sharing structure on the surface may have been very dense. Since the 2m ring is not predicted to be abundant in bulk a-SiO_2, we do not expect contributions from 2m rings to result in vibrational features such as the D_1 and D_2 defect bands in Raman spectrum, which have been shown to be correlated with a breathing mode of the 4m ring and 3m ring structure, respectively.

The density of states (DOS) for our simulated amorphous silica is given in Fig. 13. The dashed-line comes from x-ray photoemission experiments.[34] Each peak of the DOS can be characterized by the atomic nature of the corresponding electronic states in the energy region of interest. [35,36] The states above -5 eV correspond to lone pair, nonbonding $2p$ orbitals of O and the energies from -6 to -11 eV is strong bonding of Si sp^3 hybrid orbital and O p orbital. The states in the region -15 to -20 eV are primarily O $2s$ orbitals. While the DOS ranging from -5$\sim$0 eV is accurately predicted by our simulation, there is a disagreement around -10 eV peak between calculated DOS and X-ray photoemission spectra (XPS). According to Pantelides *et al.*, the disagreement between XPS and theoretical prediction is casued by matrix element effects since XPS is determined by not only valence electron density of states, but also interaction between bond orbitals at different bond site.[37] Owing to this effect, we observed the same disagreement near -10 eV peak in previous studies.[8,36]

V. CONCLUSION

In summary, we have performed *ab initio* molecular dynamics simulations for both liquid and amorphous silicon dioxide including 64 units of SiO_2 using real-space pseudopotentials. In liquid simulations, we considered liquid systems at two temperatures: 3,120 K and 3,700 K. We showed structural properties and dynamical properties at each temperature, and compared our work with previously performed Car-Parinello and classical MD simulations.

We also simulated amorphous silica. We compared several structural properties to experiments and other previous simulation results. Our calculated static structure factor reproduced the experimental data very accurately. Bond length and angle show similar values with comparing data except bond angle distribution. The differences in Si-O-Si bond angle distributions between previous work and our work are caused by a two-membered ring structure. We showed the possibility of their existence in amorphous structure not only by performing cohesive energy calculation, but also by calculating vibrational spectrum of the two-membered ring. Finally, we presented the electronic structure of amorphous silica and the results were similar to the previously performed simulation.

ACKNOWLEDGMENTS

This work is supported by U.S. Department of Energy under grant DE-SC0001878. We thank M. M. G. Alemany from Universidad de Santiago de Compostela and A. Zayak from Lawrence Berkeley National Lab for helpful discussions.

[1] A. Polman, D. C. Jacobson, D. J. Eaglesham, R. C. Kistler, and J. M. Poate, J. Appl. Phys. **70**, 3778 (1991).
[2] J.-M. Shieh, W.-C. Yu, J. Y. Huang, C.-K. Wang, B.-T. Dai, H.-Y. Jhan, C.-W. Hsu, H.-C. Kuo, F.-L. Yang, , and C.-L. Pan, Appl. Phys. Lett. **94**, 241108 (2009).
[3] Y.-n. Xu and W. Y. Ching, Phys. Rev. B **44**, 11048 (1991).
[4] F. Mauri, A. Pasquarello, B. G. Pfrommer, Y.-G. Yoon, and S. G. Louie, Phys. Rev. B **62**, R4786 (2000).
[5] S. von Alfthan, A. Kuronen, and K. Kaski, Phys. Rev. B **68**, 073203 (2003).
[6] J. P. Rino, I. Ebbsjo, R. Kalia, A. Nakano, and P. Vashishta, Phys. Rev. B **47**, 3053 (1993).
[7] T. Uchino, M. Takahashi, and T. Yoko, Phys. Rev. B **62**, 2983 (2000).
[8] J. Sarnthein, A. Pasquarello, and R. Car, Phys. Rev. B **52**, 12690 (1995).
[9] J. Sarnthein, A. Pasquarello, and R. Car, Phys. Rev. Lett. **74**, 4682 (1995).
[10] B. B. Karki, D. Bhattarai, and L. Stixrude, Phys. Rev. B **76**, 104205 (2007).
[11] M. M. G. Alemany and J. R. Chelikowsky, Phys. Rev. B **68**, 054206 (2003).
[12] J. R. Chelikowsky, J. J. Derby, V. V. Godlevsky, M. Jain, and J. Y. Raty, Journal of Physics: Condensed Matter **13**, R817 (2001).
[13] K. Vollmayr, W. Kob, and K. Binder, Phys. Rev. B **54**, 15808 (1996).
[14] Y. Zhou, Y. Saad, M. L. Tiago, and J. R. Chelikowsky, Phys. Rev. E **74**, 066704 (2006).
[15] Y. Zhou, Y. Saad, M. L. Tiago, and J. R. Chelikowsky, J. Comp. Phys. **219**, 172 (2006).
[16] K. H. Khoo, M. Kim, G. Schofield, and J. R. Chelikowsky, Phys. Rev. B **82**, 064201 (2010).
[17] K. H. Khoo, T. L. Chan, M. Kim, and J. R. Chelikowsky, Phys. Rev. B **84**, 214203 (2011).
[18] L. Kronik, A. Makmal, M. L. Tiago, M. M. G. Alemany, M. Jain, X. Huang, Y. Saad, and J. R. Chelikowsky, Phys. Stat. Sol. **243**, 1063 (2006).
[19] D. M. Ceperley and B. J. Alder, Phys. Rev. Lett. **45**, 566 (1980).
[20] N. Binggeli, J. L. Martins, and J. R. Chelikowsky, Phys. Rev. Lett. **68**, 2956 (1992).
[21] M. M. G. Alemany, R. C. Longo, L. J. Gallego, D. J. González, L. E. González, M. L. Tiago, and J. R. Chelikowsky, Phys. Rev. B **76**, 214203 (2007).
[22] J. C. Tully, G. H. Gilmer, and M. Shugard, J. Chem. Phys. **71**, 1630 (1989).
[23] L. Martin-Samos, Y. Limoge, J.-P. Crocombette, G. Roma, N. Richard, E. Anglada, and E. Artacho, Phys. Rev. B **71**, 014116 (2005).
[24] A. Carre, J. Horbach, S. Ispas, and W. Kob, Europhysics Letter **82**, 17001 (2008).
[25] A. Einstein, Annalen der Physik **17**, 549 (1905).
[26] J. R. Silva, D. G. Pinatti, C. E. Anderson, and M. L. Rudee, Philosophical Magazine **31**, 712 (1975).
[27] D. Ceresoli, M. Bernasconi, S. Iarlori, M. Parrinello, and E. Tosatti, Phys. Rev. Lett. **84**, 3887 (2000).
[28] D. R. Hamann, Phys. Rev. B **55**, 14784 (1997).
[29] T. Uchino, Y. Kitagawa, and T. Yoko, Phys. Rev. B **61**, 234 (2000).
[30] G. Boureau and S.Carniato, Solid State Comm. **98**, 485 (1996).
[31] G. Pacchioni and G. Ierano, Phys. Rev. B **56**, 7304 (1997).
[32] N. Capron, S. Carniato, A. Lagraa, G. Boureau, and A. Pasturel, J. Chem. Phys. **112**, 9543 (2000).
[33] R. D. Bendale and L. L. Hench, Surface Science **338**, 322 (1995).
[34] B. Fischer, R. A. Pollak, T. H. DiStefano, and W. D. Grobman, Phys. Rev. B **15**, 3139 (1977).
[35] J. R. Chelikowsky and M. Schüter, Phys. Rev. B **15**, 4020 (1977).
[36] R. B. Laughlin, J. D. Joannopoulos, and D. J. Chadi, Phys. Rev. B **20**, 5228 (1979).
[37] S. T. Pantelides and W. A. Harrison, Phys. Rev. B **13**, 2667 (1976).
[38] S. Susman, K. J. Volin, D. L. Price, M. Grimsditch, J. P. Rino, R. K. Kalia, P. Vashishta, G. Gwanmesia, Y. Wang, and R. C. Liebermann, Phys. Rev. B **43**, 1194 (1991).
[39] P. A. V. Johnson, A. C. Wright, and R. N. Sinclair, Journal of Non-Crystalline Solids **58**, 109 (1983).
[40] E. Dupree and R. F. Pettifer, Nature **308**, 523 (1984).
[41] P. G. Coombs, J. F. D. Natale, P. J. Hood, E. K. McElfresh, R. S. Wortman, and J. F. Schackelford, Philos. Mag. Lett. **51**, L39 (1985).
[42] A. Pasquarello, R. Car, Phys. Rev. Lett. **80**, 5145 (1998).
[43] J. M. Carpenter, D. L. Price, Phys. Rev. Lett. **54**, 441 (1985).
[44] B. A. Morrow, I. A. Cody, J. Phys. Chem. **80**, 1995 (1976).
[45] T. A. Michalske, B. C. Bunker, J. Appl. Phys. **56**, 2686 (1984).

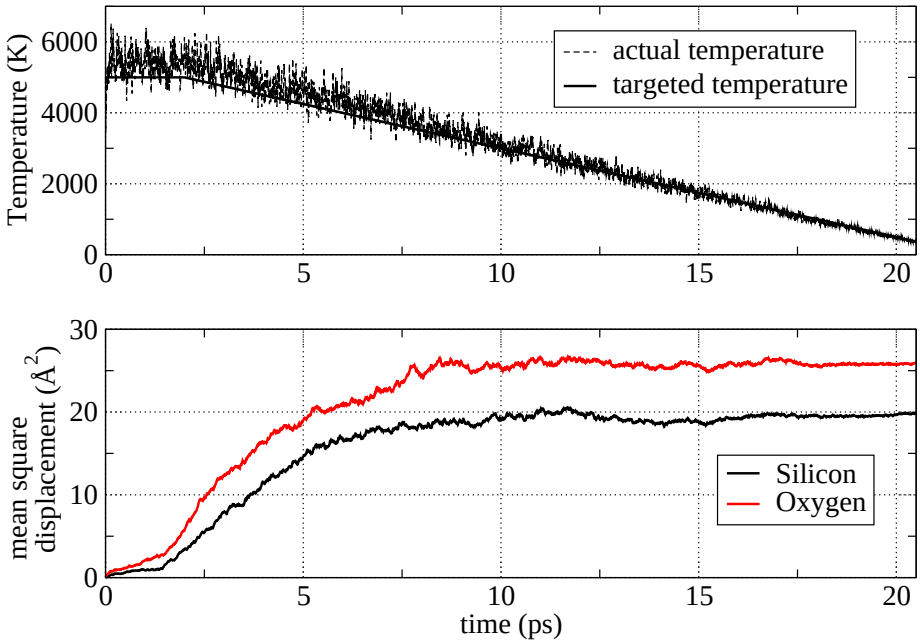

FIG. 1. Temperature(upper) and evolution of atomic mean square distances from the original position (lower) during the randomization and the annealing process of the model amorphous silica structure. Black line depicts the targeted temperature and dahsed line shows the actual temperature of the simulation box.

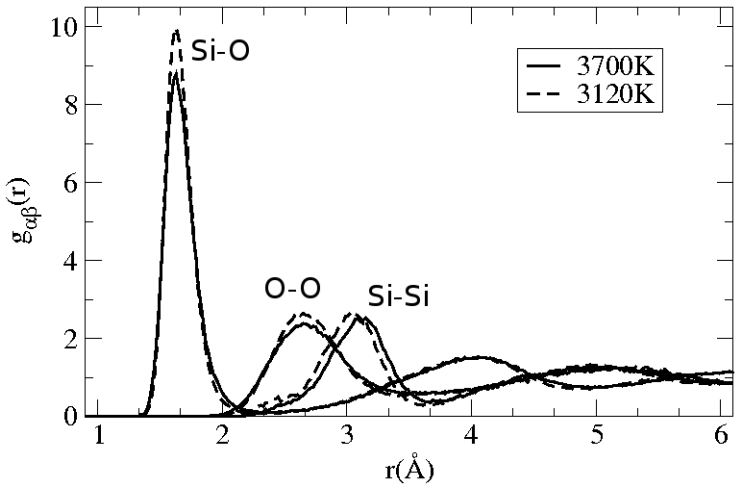

FIG. 2. Partial pair correlation function of liquid silica at 3,120 K(dashed line) and 3,700 K. The peak positions are tabulated in Table. I

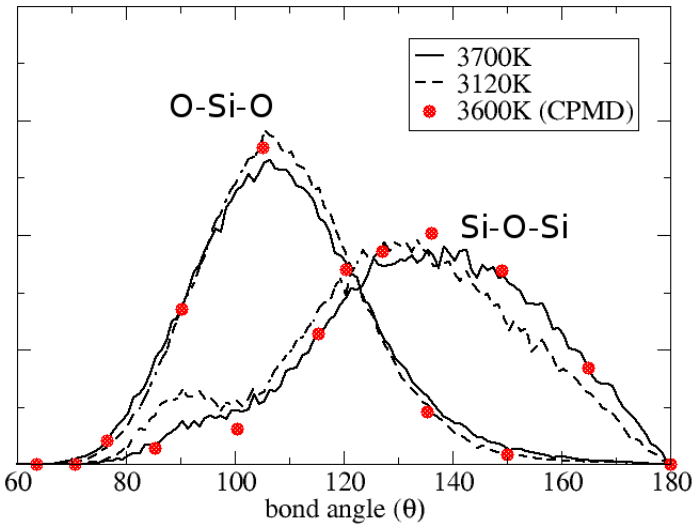

FIG. 3. Bond angle distribution function for liquid silica. 2 Å was chosen for cutoff radius. Red dots are result of 72 atoms CPMD[24] simulation.

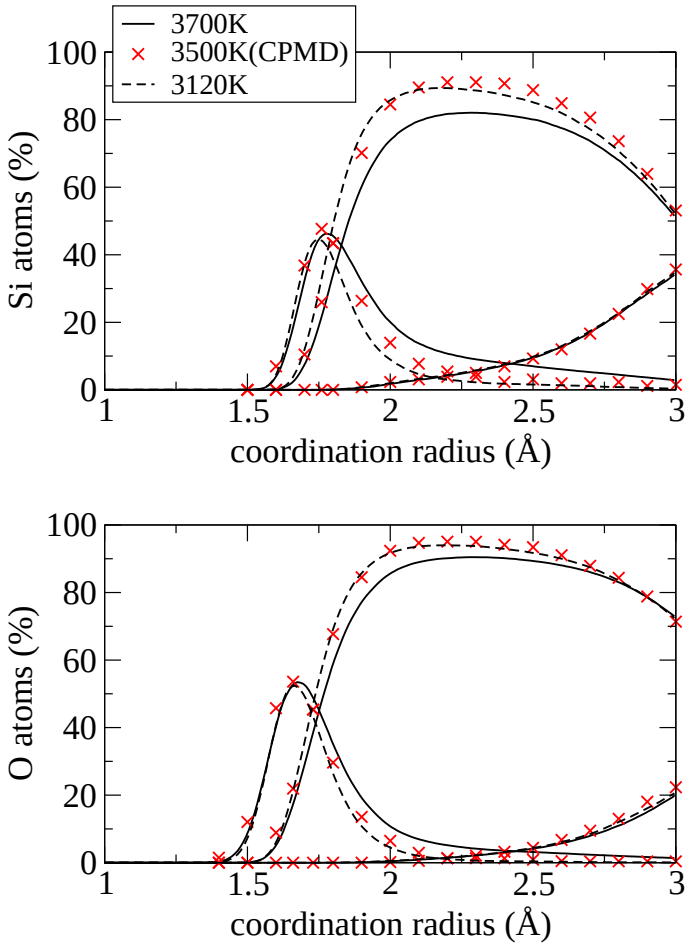

FIG. 4. Concentration of Si and O atom as a function of distance from atom center.

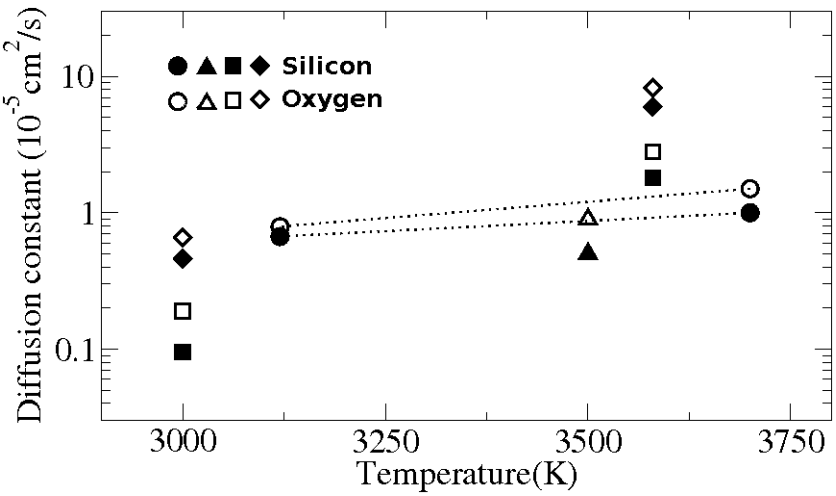

FIG. 5. Diffusion constants at various temperatures. The circles(○) indicate this work, triangles(△) are CPMD[8], diamonds(⋄) are classical CHIK potential[24], and squares(□) are classical BKS potential[24].

.

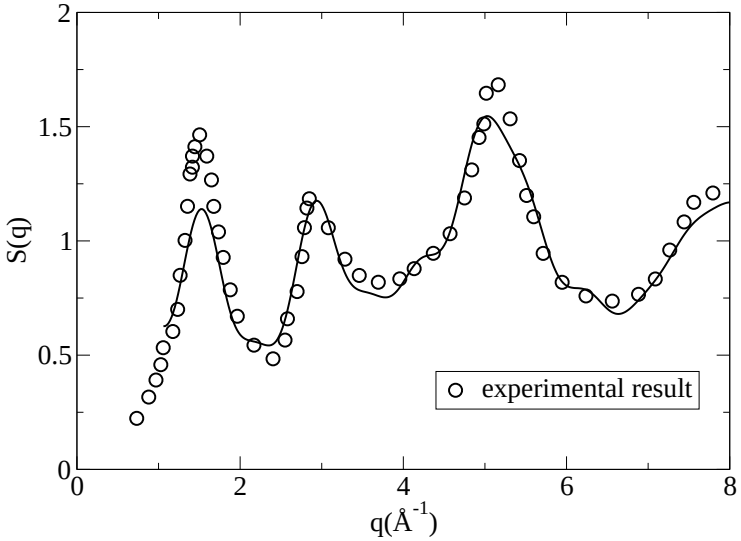

FIG. 6. Total static structure factor of amorphous silicon dioxide from a 192 atom simulation (line) and from experimental data (circles)[38].

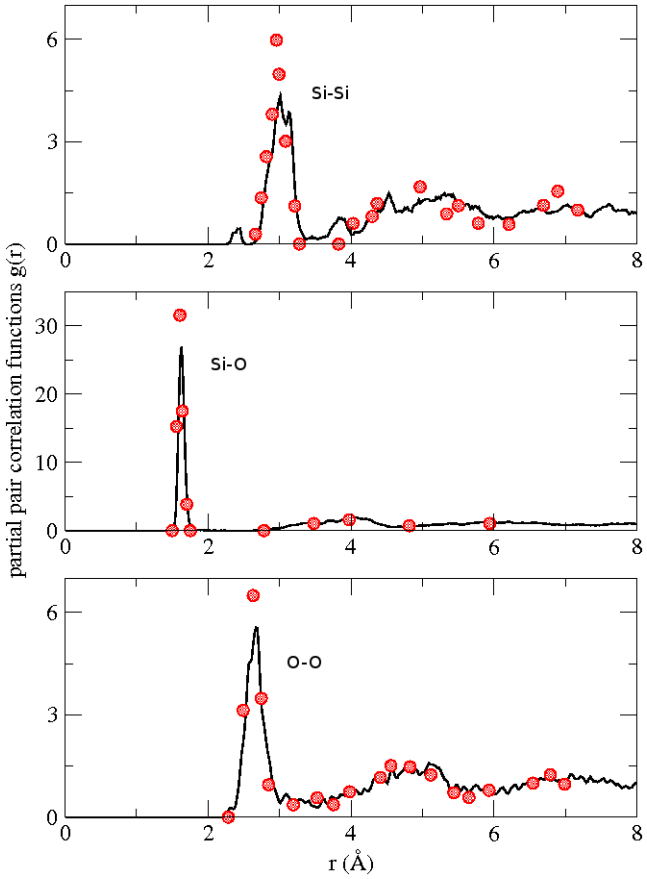

FIG. 7. Partial pair correlation function. For the comparison, several points from CPMD simulation results[8] are indicated as red dots.

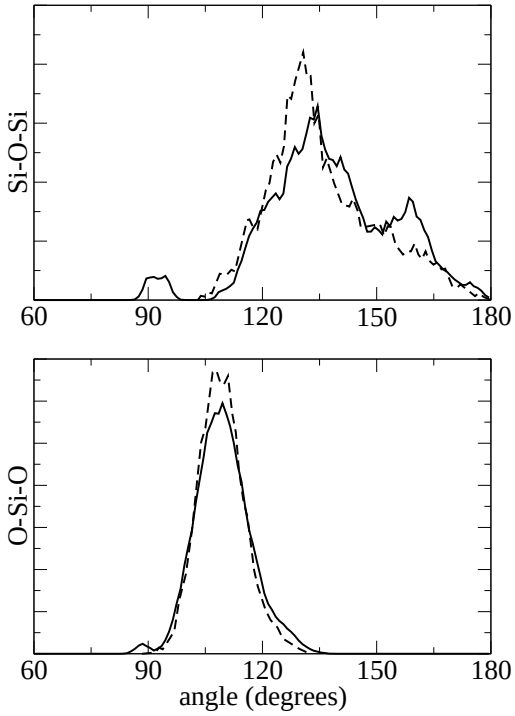

FIG. 8. Bond angle distribution function in amorphous silicon dioxide.

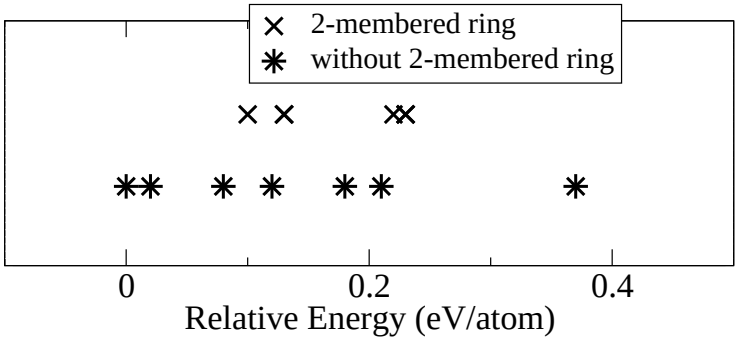

FIG. 9. Relaxed structure total energy. This graph shows the strain energy of two-membered rings do not affect to the total energy of the system.

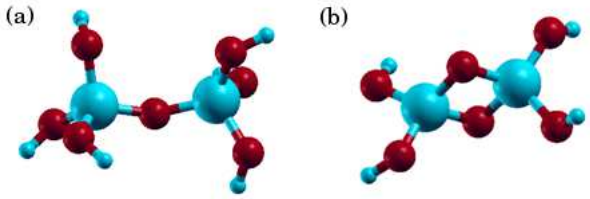

FIG. 10. Clusters used to calculate cohesive energy. (a) corner-sharing cluster. (b) two-membered ring cluster.

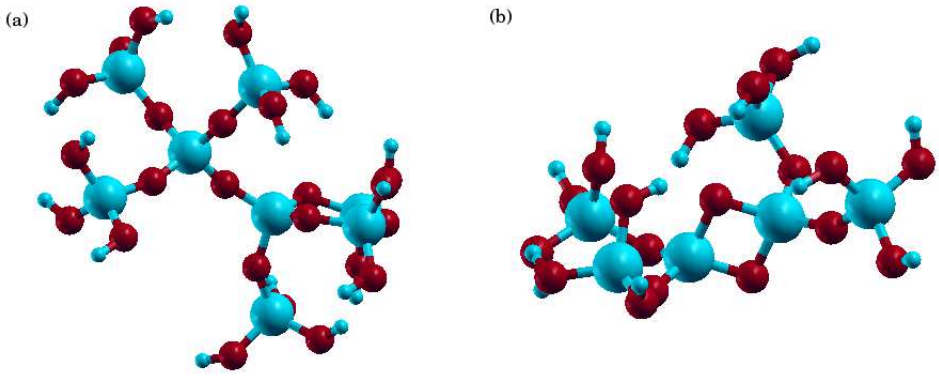

FIG. 11. One more layered cluster of Fig. 10 (a) corner-sharing cluster. (b) two-membered ring cluster.

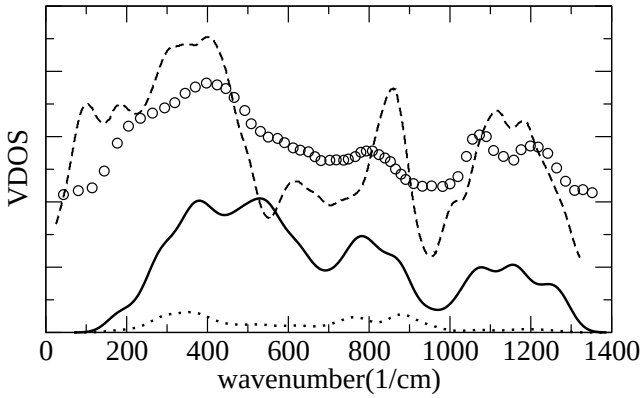

FIG. 12. The calculated vibrational density of states (solid line) and the contribution of the four atoms which constitute the two-membered ring (dotted line). 32cm^{-1} was chosen for the gaussian broadening. For the comparison, experimental data (circles) and CPMD simulation data (dashed line) were taken from Carpenter and Price[43], and Pasquarello and Car[42], respectively.

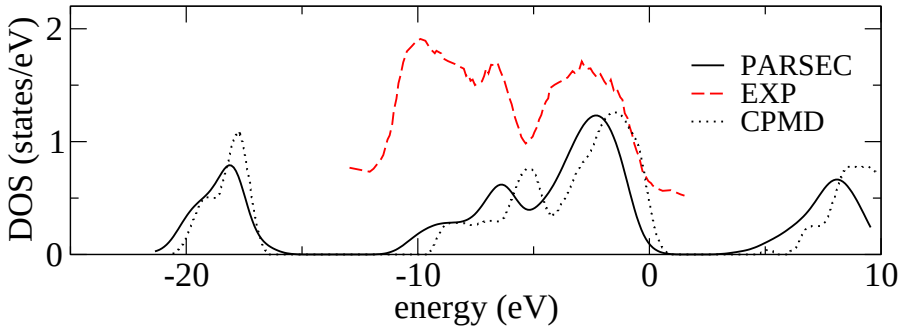

FIG. 13. Density of states of amorphous structure. The X-ray photoemission spectrum data are from Ref. 36

TABLE I. Peak positions in partial pair correlation function. (See Fig. 2) Units are Å

	Si-O			O-O			Si-Si	
	peak1	min	peak2	peak1	min	peak2	peak1	min	peak2
3700K	1.63	2.40	4.11	2.65	3.51	4.95	3.15	3.67	5.15
3120K	1.63	2.28	3.95	2.61	3.41	4.95	3.05	3.61	5.18
amorphous(300K)	1.63		4.05	2.67		5.09	3.01		5.31
β-cristobalite	1.55		3.89	2.53		4.37	3.09		5.05

TABLE II. Diffusion constants at several temperatures.

		temperature	$D_{Si}(cm^2/s)$	$D_O(cm^2/s)$	D_{Si}/D_O
ab initio MD	PARSEC	3120K	6.7×10^{-6}	7.9×10^{-6}	0.85
		3700K	1.0×10^{-5}	1.5×10^{-5}	0.67
	CPMD[a]	3500K	$5\pm1\times10^{-6}$	$9\pm1\times10^{-6}$	0.56
classical MD	BKS[b]	3000K	9.5×10^{-7}	1.9×10^{-6}	0.50
		3580K	1.8×10^{-5}	2.8×10^{-5}	0.64
	CHIK[c]	3000K	4.6×10^{-6}	6.6×10^{-6}	0.72
		3580K	6.0×10^{-5}	8.3×10^{-5}	0.72

[a] Sarnthein *et al.*[8]
[b] Carre *et al.*.[24] BKS potential
[c] Carre *et al.*.[24] CHIK potential

TABLE III. Average bond lengths and bond angles of a-SiO_2. Current work is compared Car-Parinello MD, empirical potential MD and experiments. Full width at half maximum is indicated in parenthesis.

	This work	CPMD[a]	EPMD[b]	EXP[c]
d(Si-O)	1.63 (0.09)	1.62 (0.08)	1.61 (0.08)	1.610 ±0.050
d(Si-Si)	3.01 (0.36)	2.98 (0.25)	3.07 (0.21)	3.080 ±0.100
d(O-O)	2.67 (0.26)	2.68 (0.21)	2.76 (0.25)	2.632 ±0.089
Si-O-Si	138 (24)	136 ±14	148 (27)	140-150
O-Si-O	110 (10)	109 ±6	109 (15)	109.4-109.7 (15)

[a] Ref. 9
[b] Ref. 23
[c] Refs. 26, 39, 40, and 41